RESEARCH ACTIVITIES

Photo-Molecular Science

Molecules respond to photon irradiation in a variety of ways, including photo-induced transitions and photochemical reactions. We have employed various light sources and experimental schemes to elucidate molecular structures and properties, and to control chemical reactions and molecular functions. We have also developed novel and advanced light sources for molecular science. Two of research facilities, the Laser Research Center for Molecular Science and the UVSOR Facility, conduct collaborative researches having intimate contacts with the Department of Photo-Molecular Science.

The main topics pursued in the Department include: Development of novel laser spectroscopic methods to reveal fundamental properties of molecules, development of high-resolution optical microscopic methods and application to nanomaterials, coherent control of molecules with ultrafast techniques, spectroscopy of inner-shell excited molecules and fundamental vacuum-UV photochemistry, investigation of the functionality of solid-state materials, developments of novel laser and synchrotron-orbit radiation sources, and so on.

Development of Advanced Near-Field Spectroscopy and Application to Nanometric Systems

Department of Photo-Molecular Science
Division of Photo-Molecular Science I

OKAMOTO, Hiromi	Professor
IMURA, Kohei	Assistant Professor
NARUSHIMA, Tetsuya	Assistant Professor
HORIMOTO, Noriko	IMS Fellow*
JIANG, Yuqiang	Post-Doctoral Fellow
WU, Huijun	Graduate Student
NOMURA, Emiko	Secretary

There is much demand for the study of local optical properties of molecular assemblies and materials, to understand mesoscopic phenomena and/or to construct optoelectronic devices in the nanometric scale. Scanning near-field optical microscopy (SNOM), which enables spatial resolution beyond the diffraction limit of light, has been remarkably progressed in technology in the past decade. Combination of this advanced optical technology with various nonlinear and ultrafast laser spectroscopic methods may offer a direct probe of molecular dynamical processes in mesoscopic materials systems. It may provide essential and basic knowledge for analyzing origins of characteristic features and functionalities of the mesoscopic systems. We have constructed apparatuses for near-field dynamic spectroscopy with the femtosecond time resolution and the nanometer spatial resolution. They are capable of measuring conventional near-field transmission, emission, and Raman-scattering, and unique near-field two-photon induced emission and ultrafast transient transmission as well. Based on these methods, we are observing the characteristic spatio-temporal behavior of various metal nanoparticles systems and molecular assemblies, for the purpose of understanding nano-optical characteristics, spatial coherence of excitations, dynamics, *etc*. We also investigate the basic characteristics of near-field microscopic measurements.

1. Near-Field Imaging of Locally Enhanced Optical Fields in Metal Nanoparticle Assemblies

It is of fundamental importance to reveal spatial distribution of localized optical field in metal nanostructures. In aggregated noble metal nanoparticles, for example, strong electric field is expected in the interstitial gaps between the nanoparticles, according to the electromagnetic theory. Such a localized strong optical field in the nanoparticle assembly is called as ‘hot spot’ and is considered as the major origin of the huge Raman enhancement in single-molecule level surface-enhanced Raman scattering. However, since the conventional optical microscopy is unable to resolve nanometric structures, there has been no information on the detailed structure of hot spots given by spectroscopic measurements.

In this study, we applied the near-field two-photon induced emission measurement to obtain spatial distribution of the optical fields in the vicinity of metal nanoparticle assemblies. As a result, we succeeded in clear visualization of localized intense optical fields in the assemblies of gold nanoparticles.[1)]Figure 1 shows typical topographic and near-field two-photon

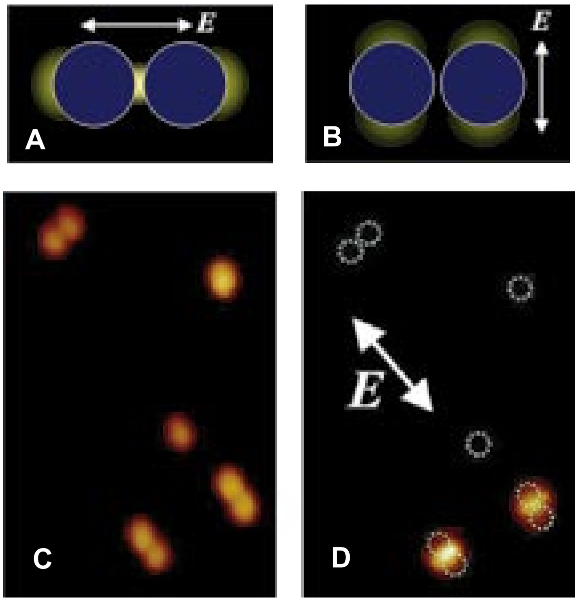

Figure 1. (A,B) Schematic view (theoretical prediction) of optical field strength in the vicinity of dimeric assemblies of metal nanospheres. The field strength is shown by the brightness. (C) Observed topography and (D) near-field two-photon excitation images of gold nanosphere (diameter 100 nm) assemblies. The dotted circles indicate positions of the nanospheres, deduced from the topography.

excitation probability images for dimeric gold nanospheres (diameter 100 nm). The two-photon image shows that the optical fields are confined at interstitial sites in the aggregates, when the incident polarization is parallel to the interparticle axes. This result agrees well with the theoretical expectations. We also performed near-field Raman imaging experiments and found that the Raman excitation is also strongly enhanced at the interstitial gaps.[1] The result gives a clear experimental proof to the hot-spot mechanism of surface-enhanced Raman scattering. In a similar way, we are examining fluorescence enhancements in the neighbor of gold nanoparticles of various shapes and their aggregates.

The methodology of visualizing the local optical field can be extensively applied to design metal nanostructures for the purpose of obtaining unique optical characteristics and/or optical fields strongly interacting with the nearby molecules. Studies in this line are under way.

2. Visualization of Plasmon Wavefunctions Induced in Various Metal Nanoparticles

We have reported that wavefunctions of localized plasmon resonances of metal nanoparticles can be visualized by using near-field transmission or two-photon excitation measurements.[2] The plasmons we visualized for chemically synthesized nanoparticles include the longitudinal modes in gold and silver nanorods and in-plane modes in gold triangular nanoplates. Figure 2 shows typical examples of near-field transmission images for longitudinal plasmon modes on a nanorod (the images correspond to the square moduli of the wavefunctions). We have reported that the images show excellent agreement with calculated images of local density of electromagnetic states which correspond to the square modulus of the resonant plasmon wavefunction.

We are extending the study to nanoparticles of other shapes and/or sizes, as well as the metal nanostructures manufactured by the electron-beam lithography technique, as a collaboration with the researchers outside of IMS. We have already obtained preliminary results for some metal nanostructures and have found peculiar plasmon waves in some cases. Such a study is also essential to design nanostructures of unique characteristics.

3. Ultrafast Transient Images of Gold Nanoparticles

We previously investigated ultrafast near-field transient transmission (space and time resolutions were *ca*. 50 nm and 100 fs) of single gold nanorods to reveal dynamic behavior of the material.[3] We used a near-infrared pulse to excite longitudinal plasmon resonance of the rod and detect transient transmission change after that. The transient image of a nanorod at *ca*. 1 ps shows characteristic features: the sign of the transient transmission change (induced or bleached) depends on the position, and the transient image contrast is sometimes reversed depending on the size of the rod.

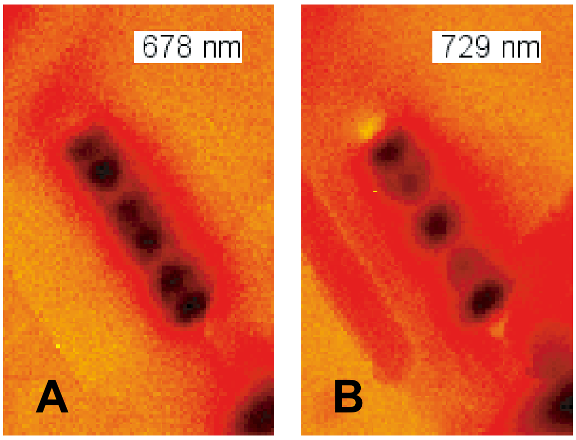

Figure 2. Near-field transmission images of a gold nanorod (diameter 20 nm, length 510 nm), observed at 678 nm (A) and 729 nm (B).

To understand the observed features, we simulated position-dependent transient transmission change based on electromagnetic density of states calculation. We have found that feature is qualitatively reproduced if we assume that the photoexcitation induces a homogeneous electronic temperature rise in the nanorod.

4. Near-Field Imaging of Organic Molecular Assemblies

We are studying mesoscopic structures and optical properties of organic molecular assemblies such as porphyrin wires, carbon nanotubes embedded in sugar molecule chains, Lagmuir-Blodgett films of functional conjugated molecules, mainly as collaborations with other research groups.

References

1) K. Imura, H. Okamoto, M. K. Hossain and M. Kitajima, *Nano Lett*. **6**, 2173–2176 (2006).
2) H. Okamoto and K. Imura, *J. Mater. Chem*. **16**, 3920–3928 (2006).
3) K. Imura, T. Nagahara and H. Okamoto, *J. Phys. Chem. B* **108**, 16344–16347 (2004).

Awards

IMURA, Kohei; The Chemical Society of Japan Award for Young Chemists.
IMURA, Kohei; Spectroscopical Society of Japan Award for Encouragement of Young Scientists.
IMURA, Kohei; Research Foundation for Opto-Science and Technology Award for Young Researchers.

* Present Address; Tohoku University, Sendai 980-8578

Quantum-State Manupulation of Molecular Motions

Department of Photo-Molecular Science
Division of Photo-Molecular Science I

OHSHIMA, Yasuhiro	Professor
HASEGAWA, Hirokazu	Assistant Professor
BAEK, Dae Yul	IMS Fellow
SUMA, Kosuke	JSPS Post-Doctoral Fellow
PAVLOV, Lubomir	Visiting Scientist*
KITANO, Kenta	Graduate Student
MIYAKE, Shinichiro	Graduate Student
INAGAKI, Itsuko	Secretary

Molecules in gas phase undergo translational, rotational and vibrational motions in a random manner, and the total molecular system is a statistical ensemble that contains a number of molecules in many different states of motions. This research group aims to establish methods to manipulate the quantum-state distribution pertinent to molecular motions, by utilizing the coherent interaction with laser lights. Here lasers with ultimate resolution in time and energy domains are employed complementally and cooperatively for manipulation of molecular motions. At the present stage, the following three subjects have been extensively explored. The first one is an exploit of impulsive interaction with ultrafast intense laser fields to achieve a nonadiabatic excitation of molecular rotation. The second subject is pertinent to creation and observation of vibrational wavepackets by fs pump–probe experiments. An experimental method newly developed in this laboratory has been applied to probing wavepackets associated with internal rotation of jet-cooled polyatomic systems. The third subject aims to realization of complete population transfer *via* an adiabatic interaction with high-resolution coherent light pulses. For this purpose, we are constructing ns laser systems, all of which are sufficiently coherent to drive the adiabatic interaction.

1. Quantum Control of Wavepacket and State Distribution *via* Nonadiabatic Rotational Excitation

When a gaseous molecular sample is irradiated by an intense nonresonant ultrafast laser pulse, the laser field exerts a torque that aligns the molecular axis along the laser polarization vector, due to the interaction with the molecular anisotropic polarizability. Because the interaction is nonadiabatic, *i.e.*, only remains in much shorter duration than the molecular rotational period, the torque is impulsive so that rotation of the molecules are excited. In a quantum mechanical point of view, this nonadiabatic rotational excitation (NAREX) creates a rotational wavepacket, a coherent superposition of rotational eigenstates.

We have recently developed a method for exploring the NAREX process in a quantum-state resolved manner by using resonance-enhanced multiphoton ionization, and reported state distribution of NO molecules, whose initial population was confined to the lowest state (J = 0.5), after the impulsive excitation with a fundamental output of a titanium-sapphire laser with ~120 fs duration.1) Population for each J after NAREX is proportional to the square of the probability amplitude of the corresponding eigenstate in the rotational wavepacket thus created. Therefore the state distribution is a useful experimental source for verifying the excitation process, and a model calculation has been performed to confirm it.

The present experimental method has been further applied to probe the state distribution after double-pulse excitation. As shown in Figure 1 (left), the population for each J changes oscillatory against the delay between the excitation pulses. Their beat patterns have been shown to provide definite information on excitation pathways in NAREX. Further theoretical consideration has proved that detailed examination in double-pulse experiments, in particular, on the population of the lowest rotational state will give rise to the full reconstruction of the rotational wavepacket even when arbitrary excitation pulses are employed. The experimental realization is now under way.

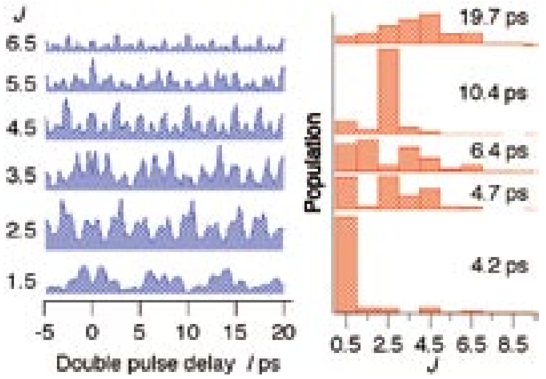

Figure 1. Population for each J state after the double-pulse NAREX against the pulse delay (left) and the corresponding state distributions at several delays (right).

Another important upshot from the double-pulse NAREX study is a partial attainment of control over rotational-state distribution with nonresonant ultrafast laser pulses. This is well demonstrated in Figure 1 (right): for instance, more than 80% of population comes back to the initial state when the delay is set to 4.2 ps, and almost 80% can be concentrated to a single eigenstate (J = 2.5, in this case) at delay of 10.4 ps. Implementation of elaborated shaping of excitation pulses is planned for further improvement in rotational-state control.

2. Wavepacket Dynamics of Methyl Internal Rotation Probed by fs Time-Resolved Fluorescence Depletion Spectroscopy

Real-time studies on low-frequency molecular vibrations with large amplitudes are of great significance, in particular, for potential application to control of isomerization reaction by coherent excitation of these motions. We have recently been exploring internal-rotation dynamics of methyl groups by utilizing ultrafast nonlinear spectroscopy, *i.e.*, fs time-resolved fluorescence depletion (fTRFD). While TRFD in ps regime has been applied previously for investigating slower intramolecular dynamics,$^{2)}$ its implementation to fs regime for vibrational wavepacket studies is for the first time. We have performed fTRFD measurements in the S_1–S_0 origin regions of several toluene derivatives in jet-cooled conditions. In particular, excitation-wavelength dependence has been examined in details for *m*-tolunitrile, as shown in Figure 2. Here the quantum interferences for the A_1 and E symmetry levels in both the S_0 and S_1 states are clearly observed. Beat components for each levels change their magnitudes for different excitation wavelengths. These dependences have been analyzed with model calculations numerically solving the time-dependent Liouville equations for methyl internal rotation. Comparison of the observed fTRFD spectra with the calculated results shows that ca. 10% of population is transferred to the S_1 manifold in the present condition.

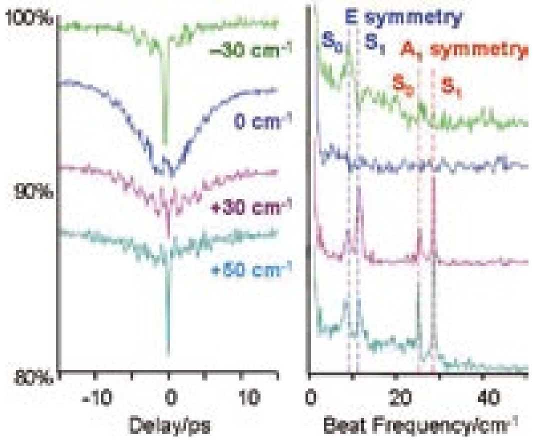

Figure 2. fTRFD spectra for different excitation wavelengths, indicated as offset wavenumbers from the origin band (left) and the corresponding power spectra (right).

3. Construction of Coherent ns Pulsed Light Sources for Adiabatic Population Transfer

Highly efficient population transfer between quantum states can be accomplished with adiabatic interactions with ns coherent laser pulses, such as stimulated Raman adiabatic passage.$^{3)}$ For realizing such an adiabatic quantum-state manipulation, we are constructing two independent laser systems, both of which will deliver pulsed outputs with almost Fourier-transform (FT) limited resolution. The first system, already in operation, is based on the pulsed amplification of the output from a cw ring titanium-sapphire laser. The third harmonics of the pulsed laser system has been applied for recording high-resolution excitation spectrum of the S_1–S_0 6_0^1 band of jet-cooled benzene (Figure 3). Spectral Linewidth (0.013 cm^{-1}) of single ro-vibronic transitions is three times of FT limit. The second laser system is based on the optical parametric oscillation (OPO) injection-seeded by an extra-cavity cw diode laser. Quite recently, we have succeeded in single-mode operation of the OPO system, in which only a few mW of the cw light is necessary for stable injection seeding. The optical layout is now optimized for further increment of the output power up to the level sufficient for driving adiabatic population transfer.

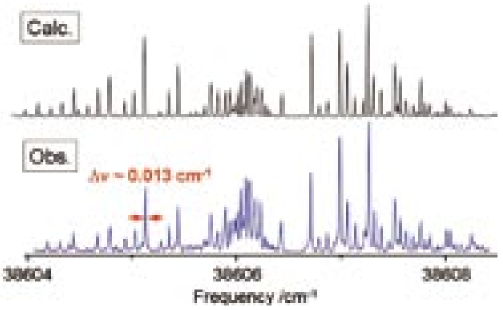

Figure 3. High-resolution excitation spectrum of benzene S_1–S_0 6_0^1 band. Rotational temperature is set to 2 K for simulation.

References

1) H. Hasegawa and Y. Ohshima, *Phys. Rev. A* **74**, 061401 (4 pages) (2006).
2) M. J. Côté, J. F. Kauffman, P. G. Smith and J. D. McDonald, *J. Chem. Phys.* **90**, 2865–2873 (1989); G. V. Hartland, L. L. Connell and P. M. Felker, *J. Chem. Phys.* **94**, 7649–7666 (1991).
3) N. V. Vitanov, T. Halfmann, B. W. Shore and .K. Bergmann, *Annu. Rev. Phys. Chem.* **52**, 763–809 (2001).

Award

KITANO, Kenta; Best Poster Presentation Award in 23rd Symposium on Chemical Kinetics and Dynamics.

---

* from Bulgarian Academy of Science

Development of High-Precision Coherent Control and Its Applications

Department of Photo-Molecular Science
Division of Photo-Molecular Science II

OHMORI, Kenji	Professor
KATSUKI, Hiroyuki	Assistant Professor
HOSAKA, Kouichi	IMS Fellow
DELAGNES, Jean-Christophe	Post-Doctoral Fellow*
SHIMADA, Hiroyuki	Post-Doctoral Fellow
GOTO, Haruka	Graduate Student
INAGAKI, Itsuko	Secretary

Coherent control is based on manipulation of quantum phases of wave functions. It is a basic scheme of controlling a variety of quantum systems from simple atoms to nanostructures with possible applications to novel quantum technologies such as bond-selective chemistry and quantum computation. Coherent control is thus currently one of the principal subjects of various fields of science and technology such as atomic and molecular physics, solid-state physics, quantum electronics, and information science and technology. One promising strategy to carry out coherent control is to use coherent light to modulate a matter wave with its optical phase. We have so far developed a high-precision wave-packet interferometry by stabilizing the relative quantum phase of the two molecular wave packets generated by a pair of femtosecond laser pulses on the attosecond time scale. We will apply our high-precision quantum interferometry to gas, liquid, solid, and surface systems to explore and control various quantum phenomena.

1. READ and WRITE Amplitude and Phase Information by Using High-Precision Molecular Wave-Packet Interferometry[1)]

We demonstrate an experimental approach to read and write populations and relative phases of vibrational eigenstates within a wave packet created in the *B* state of the iodine molecule by using a pair of phase-locked femtosecond laser pulses. Our highly-stabilized optical interferometer keeps attosecond stability and resolution in the interpulse delay. These stability and resolution have realized an exquisite tuning of the interference of two vibrational wave packets to manipulate the relative populations and the relative quantum phases among the relevant vibrational eigenstates. These populations and phases have been retrieved by measuring fluorescence from the upper *E* state induced by another nanosecond (ns) or femtosecond (fs) probe laser pulse. The bandwidth of the ns probe pulse is narrow enough to select only a small portion of the rotational progression of a particular vibrational band of the *E*–*B* transition. By scanning the probe wavelength, we measure the population distribution of the vibrational eigenstates within the wave packet. The fs probe pulse is used to measure quantum beats arising from the temporal evolution of the wave packet. Combining these two complementary measurements, we can read both population and phase information written and stored in the wave packet.

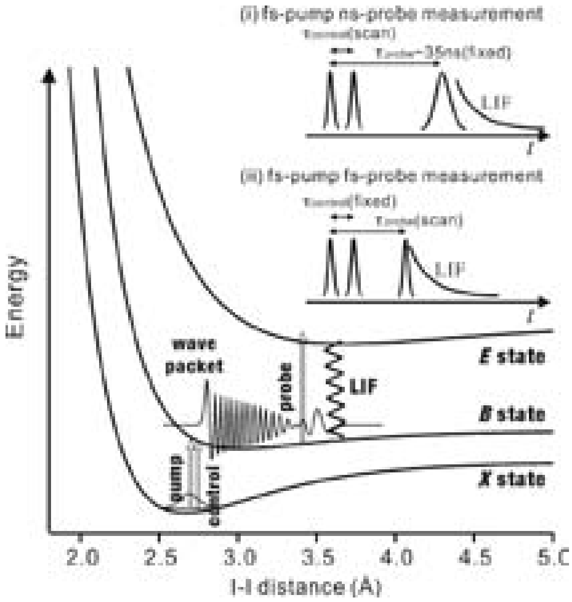

Figure 1. Pump-control-probe scheme for the real-time or state-resolved measurement of wave-packet interference with the femtosecond or nanosecond probe pulse. The potentials are only schematic.

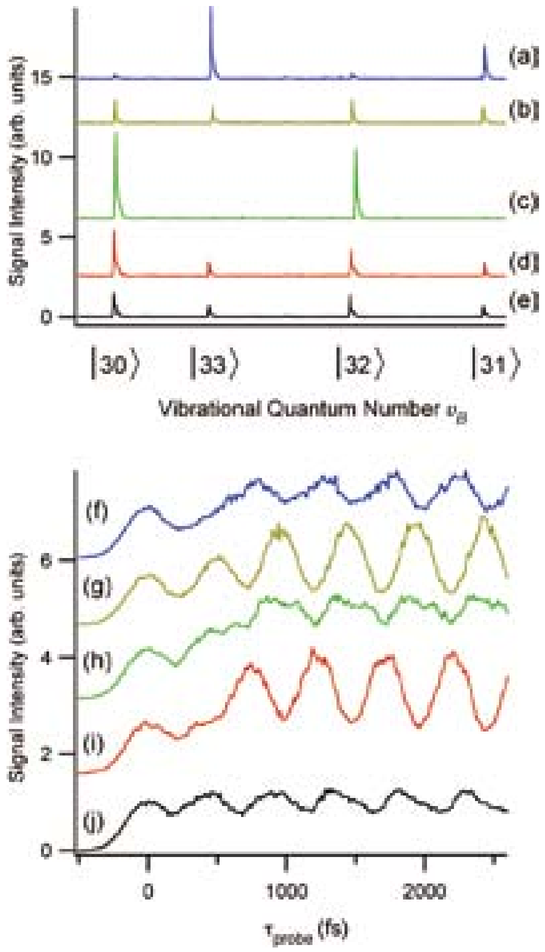

Figure 2. Wave packet interference measured with the pump and control delay $\tau_{control}$ tuned to ~(1+1/2) T_{vib} (~760 fs), where T_{vib} is a classical vibrational period of I_2. (a)–(d) “POPULATION CODES” measured by scanning the wavelength of the ns probe pulse. The relative phase θ_{p-c} of the pump and control pulses is increased in steps of ~π/2 in going from (a) to (d). (e) Population code written without the control pulse and displayed for reference. The five population codes are displaced vertically from one another for clarity. (f)–(i) “PHASE CODES” measured with almost the same θ_{p-c}’s as for (a)–(d), respectively. (j) Phase code written without the control pulse and displayed for reference. The five phase codes are displaced vertically from one another for clarity. A possible deviation of θ_{p-c} within each set of the population and phase codes is estimated to be < 0.2π for the sets (a)–(f) and (c)–(h), and < 0.03π for (b)–(g) and (d)–(i).

Reference

1) H. Katsuki, K. Hosaka, H. Chiba and K. Ohmori, *Phys. Rev. A* **76**, 013403 (13 pages) (2007).

Awards

OHMORI, Kenji; Japan Academy Medal.
OHMORI, Kenji; JSPS Prize.

* Present Affiliation; Senior Lecturer, The University of Bordeaux, France

Molecular Inner-Shell Spectroscopy: Electronic Structure and Intermolecular Interaction

Department of Photo-Molecular Science
Division of Photo-Molecular Science III

KOSUGI, Nobuhiro	Professor
HATSUI, Takaki	Assistant Professor
NAGASAKA, Masanari	Assistant Professor
KIMBERG, Victor	JSPS Post-Doctoral Fellow
NAKANE, Junko	Secretary

To reveal electronic structure and intermolecular interaction of free molecules and molecular solids and clusters, we are developing and improving soft X-ray spectrometers for resonant photoelectron spectroscopy and inelastic soft X-ray emission spectroscopy optimized to an undulator beamline BL3U at the UVSOR facility. We are also developing and improving an original *ab initio* quantum chemical program package GSCF, which is optimized to calculation of molecular inner-shell processes.

1. High-Resolution Soft X-Ray Emission Spectroscopy with a Transmission Grating

We have recently reported our new design of a transmission-grating spectrometer (TGS) for high resolution soft X-ray emission studies.1) The high resolution spectrometer generally requires high light gathering capability without sacrificing the energy resolution. This requirement can be fulfilled by use of the Wolter type-I mirror and the transmission grating (TG). Our spectrometer incorporates the basic concept for x-ray imaging and spectroscopy telescopes2) into a compact and easy-to-use layout.

The present optical layout is a modification of the Rowland torus mount with facet gratings. In the ideal Rowland torus mount, the facet TGs should be mounted onto Rowland torus with keeping their normal to point the focus of the incoming x-rays. In our spectrometer, the facet TGs are positioned onto a single Si wafer. Such simplification might degrade optical properties. However, we demonstrated by ray-tracing simulations that the aberration in our geometry is small enough to realize the energy resolving power better than 5000.

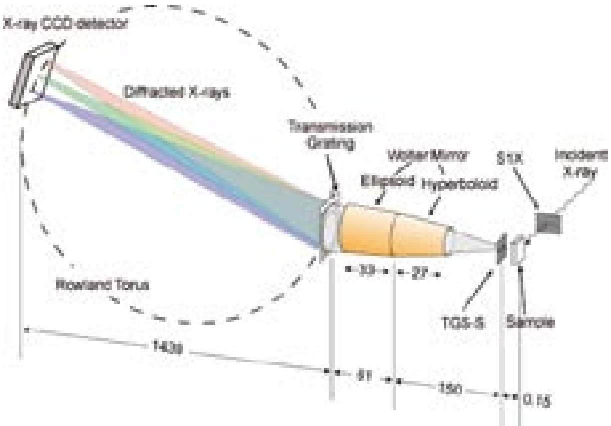

Figure 1. Layout of the present soft X-ray emission spectrometer.

Our TGS shown in Figure 1 is installed at the XES end-station of the undulator beamline BL3U. A soft x-ray emission spectrometer generally requires small beam size at the sample position, because a smaller opening of the spectrometer entrance slit is needed to achieve higher energy resolution. BL3U is designed to give small beam size of order of 10 × 40 μm^2. To check the stray light contamination, the profile of the 0th order diffraction was measured. The stray light intensity was less than 1% of the 1st diffraction order intensity. To check the energy resolution, diffuse scattering from aluminum samples illuminated by 60 eV soft x-rays was measured. Figure 2 shows the 1st order diffraction peak. The peak width was FWHM of 3 pixels, which corresponds to the energy resolving power of 4600. To our knowledge, the present resolving power is more than 4 times higher than the best record reported so far.

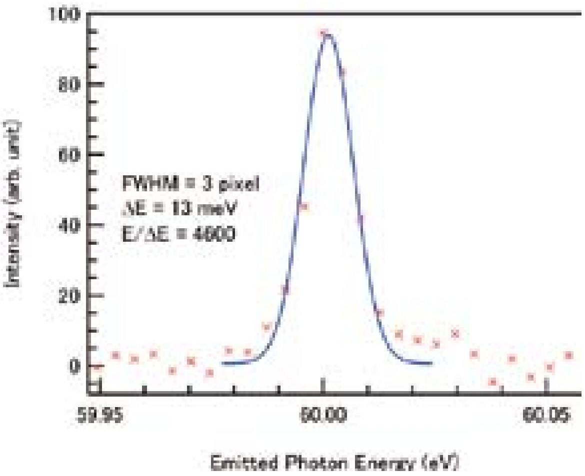

Figure 2. 1st order diffraction peak of the diffuse scattering from aluminum samples ($h\nu$ = 60 eV), observed by using the present TGS.

2. X-Ray Natural Circular Dichroism of Amino Acids[3)]

X-ray absorption spectroscopy (XAS) is a powerful tool to study even large molecules. Due to the localized character of a core electron responsible for XAS, it is possible to correlate a specific XAS feature with a specific functional group or with an individual bond. In addition, even natural circular dichroism (NCD) is now observable in XAS of amino acids, though difference in XAS between the left and right circularly polarized X-rays proves to be tiny : $g = 2(I_L–I_R)/(I_L+I_R) \approx 10^{–3}$.

In the present work, we evaluate feasibility of different theoretical approaches for XNCD by using GSCF3 and other available *ab initio* codes. We describe the excited orbital set using the ground state Hartree-Fock (HF) orbital set employed in (i) RPA and (ii) static exchange approach (STEX) (unrelaxed), (iii) core-ionized state HF orbital set applied in STEX(relaxed) and (iv) HF excited state orbital set for each core-to-valence excited state. Furthermore in (i) the DFT-RPA method is compared with the RPA where the *ab initio* HF orbital set is used. In (iv), the oscillator and rotary strengths evaluated by different orbital sets for the initial and final states, namely, non-orthogonal ground-state and core-excited HF orbitals, are compared with those evaluated by using the core-excited HF orbital set to describe the initial (ground) state.

The basis set dependence of XNCD spectra of some amino acids in different approaches is systematically investigated using Woon and Dunning basis sets up to aug-cc-pCV5Z. The RPA calculation shows most satisfactory and self-consistent results for the low-lying core-to-valence excitations near the O K-edge. A clear convergence of the oscillator strength for the basis sets larger than triple-zeta is found for the RPA approach. Use of extended quadruple-zeta or larger basis sets are required to obtain satisfactory results for the rotary strength on the O K-edge. The relative simplicity of the RPA technique using the same ground-state HF orbital set for any core-to-valence excitation makes it applicable to chiral centers in rather large compounds such as proteins.

3. Inner-Shell Ionized and Excited States of Molecular Pyridine Clusters[4)]

Photoionization of clusters containing aromatic molecules shows characteristic redshifts of the appearance energies in the regime of the first ionization energy.[5)] These redshifts are rationalized with the polarization (PL) effect by molecules surrounding a positively-charged core-ionized molecule. On the other hand, photoexcitation of clusters containing aromatic molecules does not show such a PL effect, because the core excited states are neutral. Recently, we have investigated the C 1s–π* excitation in variable size benzene clusters,[6)] whose excited states undergo substantial redshifts up to 60 meV relative to the isolated molecule. On the other hand, the N 1s–π* excitations in pyridine clusters show ca. 60 meV-blueshifts. The mechanism of the energy shift in inner-shell excitation of molecular clusters could be different from that in inner-shell ionization.

The most stable pyridine dimer structure is theoretically found to be an anti-parallel displaced structure with the N atoms opposing each other, where the positively charged H atom of one ring lies on top of the negatively charged nitrogen atom of the other ring. In the parallel displaced geometry of pyridine trimer, the middle pyridine is displaced with respect to the top and bottom pyridine rings, such as two anti-parallel displaced pyridine geometries. In contrast to less stable parallel displaced stacking interaction in benzene dimer, the stacking interaction in pyridine dimer and trimer is stabilized electrostatically with the permanent dipole moment.

In the anti-parallel displaced dimer structure the blueshift is calculated to be 42 meV by using GSCF3. In the anti-parallel displaced trimer, the N 1s on the middle ring has the largest blueshift of 85 meV, whereas the top and bottom N 1s leads to the same blueshift of 42 meV as in the dimer. This means the second neighbor molecule is not contributive at all to the energy shift. We have also observed that the N 1s–π* excitation energy shift is oscillating against a horizontal sliding in the anti-parallel displaced pyridine dimer. This indicates covalent intermolecular interaction is important; that is, a small π–π orbital interaction is visible as a small energy shift in the 1s–π* excitation even in van der Waals clusters. In addition, this result indicates a possibility to know nearest neighbor molecular conformation by referring to the shift in core-to-valence excitation energy.

References

1) T. Hatsui, E. Shigemasa and N. Kosugi, *J. Electron Spectrosc. Relat. Phenom.* **144**, 1059 (2005).
2) K. P. Beuermann, H. Bräuninger and J. Trümper, *Appl. Opt.* **17**, 2304 (1978).
3) V. Kimberg and N. Kosugi, *J. Chem. Phys.* **126**, 245101 (2007).
4) I. Bradeanu and N. Kosugi, *AIP Conf. Proc.* **882**, 815 (2007).
5) E. Rühl, P. Bisling, B. Brutschy and H. Baumgärtel, *Chem. Phys. Lett.* **126**, 232 (1986).
6) I. L. Bradeanu, R. Flesch, N. Kosugi, A. Pavlychev and E. Rühl, *Phys. Chem. Chem. Phys.* **8**, 1906 (2006).

Extreme UV Photoionization Studies of Fullerenes by Using Synchrotron Radiation and High-Temperature Mass Spectrometer

Department of Photo-Molecular Science
Division of Photo-Molecular Science III

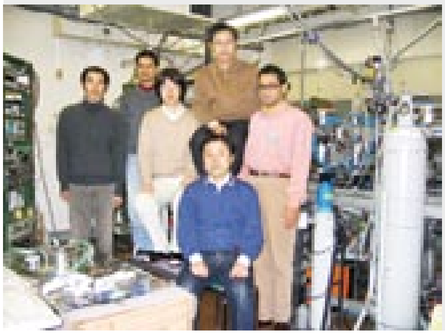

MITSUKE, Koichiro	Associate Professor
KATAYANAGI, Hideki	Assistant Professor
HUANG, Chaoqun	IMS Fellow
YAGI, Hajime	Post-Doctoral Fellow
KAFLE, Bhim Prasad	Graduate Student
PRODHAN, Md. Serajul Islam	Graduate Student

The interactions of C_{60}, C_{70}, C_{84} … with high-energy photons have attracted considerable attention, since fullerenes provide unique molecular systems characterized by exceptionally stable electronic structures associated with dense and highly degenerated molecular orbitals and by extremely large vibrational degrees of freedom. In UVSOR we have investigated the yield curves of singly- and multiply-charged photoions from fullerenes by using a grazing incidence monochromator in the $h\nu$ range from 25 to 200 eV. We succeeded in absolutizing the partial and total photoionization cross section curves of $C_{60(70)}$. Moreover, we have measured the yield curves for $C_{60(70)-2n}{}^{z+}$ from $C_{60(70)}$ as a function of the internal energy of the parent $C_{60(70)}{}^{z+}$ ions to study the mechanisms and kinetics of sequential C_2-release reactions.

1. Relative Partial Cross Sections for Single, Double and Triple Photoionization of C_{60} and C_{70}[1)]

Partial cross sections for the photoion formation from C_{60} and C_{70} were determined from the yields of singly, doubly and triply charged ions at $h\nu$ = 25–120 eV. The dependence of the detection efficiencies on the mass-to-charge ratio was evaluated by using the formula proposed by Twerenbold *et al.* Corrections of the detection efficiency were found to be critical to obtain accurate partial cross sections. Revisions were made of the partial cross-section curves for single and double photoionization of C_{60} and C_{70}. The curve for triple photoionization of C_{70} was newly proposed. The ratios between the cross sections for double and single photoionization increase with $h\nu$ and reach saturated values of 0.78 at 85 eV for C_{60} and ~1.3 at 100 eV for C_{70}. In contrast, the ratios at 120 eV between the cross sections for triple and single photoionization of C_{60} and C_{70} amount to be 0.14 and ~0.38, respectively. Formation mechanism of multiply-charged fullerene ions was discussed in terms of valence-electron excitation to antibonding unoccupied orbitals and/or spherical standing waves inside the cavity of a fullerene. This excitation could be followed by Spectator Auger processes and transmission of the excess electronic energy among numerous vibrational degrees of freedom.

2. Absolute Total Photoionization Cross Section of C_{60} in the Range of 25–120 eV[2)]

The absolute total photoionization cross section of C_{60} has been measured at $h\nu$ = 25–120 eV. Evaluation has been made on the detection efficiency of fullerene ions in different charge states. The present total photoionization cross section curve has been combined with the absorption cross section curves of C_{60} at $h\nu$ = 3.5–26 eV in the literature, after appropriate alterations of the vapor pressure being taken into account. The oscillator strengths are calculated from the combined cross section curve to be 230.5 and 178.5 at $h\nu$ = 3.5–119 and 3.5–40.8 eV, respectively. These oscillator strengths agree well with those expected from the TKR sum rule. Moreover, the total photoionization cross section curve of the present study is

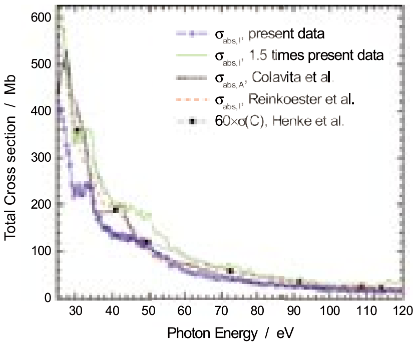

Figure 1. ○, total photoionization cross section $\sigma_{abs,I}$ of C_{60} of the present study; —, $\sigma_{abs,I}$ of the present study multiplied by 1.5; --, experimental $\sigma_{abs,I}$ by Reinköster *et al.*; ▬, theoretical total photoabsorption cross section $\sigma_{abs,A}$ by Colavita *et al.*; ■, 60 times $\sigma_{abs,A}$ of a C atom by Henke *et al.*

consistent with those of recent experimental and theoretical studies (see Figure 1).

3. Relative Partial Cross Sections for Single, Double and Triple Photoionization of C_{84}

The partial cross sections for the photoion formation from C_{84} were newly determined from the yields of singly, doubly and triply charged ions at $h\nu$ = 55–120 eV. The ratios between the cross sections for double and single photoionization increase with $h\nu$ and reach saturated values of ~0.9 at 80 eV. In contrast, the ratios at 120 eV between the cross sections for triple and single photoionization amount to be ~0.18, respectively.

4. Kinetic Energy Analysis of the Fragment Ions Produced from C_{60} and C_{70}[3)]

We reported the yield curves of the fragments $C_{60-2n}{}^{z+}$ and $C_{70-2n}{}^{z+}$ ($n \geq 1$, $z \geq 1$) produced from C_{60} and C_{70}, respectively, at $h\nu$ = 45–150 eV. Then the mechanism of sequential loss of C_2 units has been proposed on a basis of comparison between the experimental ion yield curves and theoretical fractional abundance curves. The latter curves have been derived by employing the RRKM theory to individual unimolecular reactions, $C_{60-2n+2}{}^{z+} \rightarrow C_{60-2n}{}^{z+} + C_2$. More reliable calculations of the rate constants of these reactions are needed before closer comparison between the two curves. For such calculations we should know precise values of the activation energies for the reactions, together with the vibrational spectra of the transition states. This induced us to develop a new spectrometer for the fragment ions. It is likely that the magnitude of the potential barriers can be estimated from the average kinetic energy release measured by this spectrometer.

5. Scattering Distributions of the Photofragments from Fullerenes

We are developing an imaging spectrometer to measure the three-dimensional momentum distributions of the ionic photofragments produced from fullerenes at $h\nu > 50$ eV. High kinetic-energy resolution is expected to be achieved on the images by adopting the Eppink-Parker type velocity focusing lens system. We will be able to distinguish the two possible mechanisms of fragmentation of fullerene ions, *i.e*. stepwise C_2 ejection and direct fission into two species, since different momentum distributions result in different projected images on the position sensitive detector.

6. ZEKE Photoelectron Spectroscopy Using the Dark Gap of the Storage Ring

We have constructed a threshold photoelectron spectrometer for the purpose of measuring the signal of threshold electron-photoion coincidence (TEPICO), using the dark gap of the UVSOR facility. Such measurements provide us with the detailed information about the excitation/de-excitation and decay processes of C_{60} and C_{70}. We already succeeded in observing the electron signal from He and O_2 samples, but the spectra suffered from intense background counts. The background needs to be reduced to the utmost for performing the TEPICO measurement. It is also necessary to improve the efficiency of the spectrometer for threshold electrons. We are therefore developing an improved version of the spectrometer which has the capability to significantly reject the electrons with high kinetic energies and to guide slow electrons (KE = 0 to 10 meV) to the detector.

7. High Resolution Photoelectron Spectroscopy of Gaseous C_{60}

Photoelectron spectroscopy (PES) of solid C_{60} has been performed by several groups to clarify its electronic structure. However, comprehensive PES studies of gaseous C_{60} are few and the energy resolution was ~100 meV at the best. This resolution was not enough to distinguish closely spaced bands, though many degenerate bands are located in the 7–40 eV ionization energy range. We are developing an apparatus of high-resolution angle-resolved PES. Our goal is to carry out PES of various kinds of fullerenes with a total energy resolution of ~20 meV at the UVSOR facility. The partial photoionization cross section and anisotropy parameter of each band are expected to be determined at $h\nu$ = 25–150 eV.

8. Photodissociation of Butyl Cyanides and Butyl Isocyanides[4)]

Photodissociation process to produce the electronically excited $CN(B\Sigma^+)$ fragment has been studied for four structural isomers, n-C_4H_9CN, t-C_4H_9CN, n-C_4H_9NC and t-C_4H_9NC by using synchrotron radiation. Photoexcitation spectra for the $CN(B^2\Sigma^+ \rightarrow X^2\Sigma^+)$ transition were measured in the excitation wavelength range of 85–165 nm (7.5–14.5 eV) and the CN $(B^2\Sigma^+ \rightarrow X^2\Sigma^+)$ emission spectra were dispersed at several wavelengths in the range of 57–140 nm. Quantum yields for the production of the CN(B) state from photodissociative excitation of the isocyanides were larger than those from the cyanides. The quantum yields from the molecules consisting of a *tertiary*-butyl group were larger than those from the *normal*-butyl compounds.

References

1) K. Mitsuke, H. Katayanagi, C. Huang, B. P. Kafle, Md. S. I. Prodhan, H. Yagi and Y. Kubozono, *J. Phys. Chem. A* **111**, 8336–8343 (2007).

2) B. P. Kafle, H. Katayanagi, Md. S. I. Prodhan, H. Yagi, C. Huang and K. Mitsuke, *J. Phys. Soc. Jpn*. submitted.

3) B. P. Kafle, H. Katayanagi and K. Mitsuke, *AIP Conf. Proc*. **879**, 1809–1812 (2007).

4) K. Kanda, K. Mitsuke, K. Suzuki and T. Ibuki, *AIP Conf. Proc*. **879**, 1817–1820 (2007).

Molecules in Few-Cycle Intense Laser Fields

Department of Photo-Molecular Science
Division of Photo-Molecular Science III

HISHIKAWA, Akiyoshi	Associate Professor
FUSHITANI, Mizuho	Assistant Professor
MATSUDA, Akitaka	IMS Fellow
NAKANE, Junko	Secretary

When exposed to intense laser fields, molecules exhibit a variety of exotic features as the magnitude of the electric field component is comparable with that of the Coulomb field within a molecule. For a deeper understanding of the light-matter interaction, we investigate how atoms and molecules behave in strong and ultrashort laser fields, which carry only a few optical cycles within the pulse.

1. Electronic and Nuclear Responses of Fixed-in-Space H_2S to Ultrashort Intense Laser Fields[1)]

The Coulomb explosion dynamics in non-resonant, ultrashort intense laser fields (12 fs, ~10^{14} W/cm^2) is studied for H_2S with its orientation fixed in space, to clarify how the electronic and nuclear responses change by the direction of laser polarization direction (ε) in the molecular frame (Figure 1). The momenta of the respective fragment ions, $p_1(H^+)$, $p_2(H^+)$ and $p_3(S^+)$ produced in the Coulomb explosion process, $H_2S^{3+} \rightarrow H^+ + S^+ + H^+$, were determined as three-dimensional vectors in the laboratory frame. The kinetic energy release (E_{kin}) and momentum angle (θ_{12}) distributions obtained for the respective directions revealed that the geometrical structure is almost frozen during the interaction with the laser fields for $x//\varepsilon$, while it becomes elongated along the laser polarization vector when ε is parallel to the y- or z- axis, demonstrating that the Coulomb explosion dynamics of H_2S in intense laser fields can be manipulated by the polarization direction in the molecular frame.

The elongation in the molecular structure can be interpreted in terms of the induced dipole potential, $U_{id} = -\alpha\varepsilon^2/2$. As the molecular structure stretches along ε, the corresponding component of polarizability tensor α becomes larger, which lowers the potential energy to induce the nuclear dynamics towards the elongated structures. Alternatively, the observed structural deformation can be explained by the population transfer to charge transfer (CT) states characterized with the ionic charge distribution and the large transition moments from the ground state. Because of the ionic character, CT states can be stabilized in intense laser fields against the covalent ground state when the direction of the charge separation is parallel to the electric field ε. The large transition moments then facilitates the laser induced non-adiabatic population transfer from the ground state to the CT state, which leads to the enhanced ionization and dissociation in intense laser fields by the localized charge distribution.

In the case of H_2S, CT states with the H^-–S–H^+ (and H^+–S–H^-) type configuration and those with the H_2^+–S^- or H_2^-–S^+ character are expected to contribute to the dynamical processes for the $y//\varepsilon$ and $z//\varepsilon$ directions, respectively. Possible candidates of such CT (ionic) states are the electronically excited 3^1B_2 and 5^1A_1 states located at 13.9 eV and 13.7 eV above the ground state at the equilibrium geometry. The transition moments from the ground state, X^1A_1 , are $|\mu|$ = 1.57 and 1.34 a.u., along the y- and z-axis, respectively.

On the other hand, no such CT states can be coupled with the ground state when ε is perpendicular to the molecular plane. The ionization process for $x//\varepsilon$ should be dominated by the tunneling ionization from the HOMO $2b_1$ extending perpendicular to the plane. The ionized electron is then rescattered by the ion core to form highly charged parent ions within a few optical cycles, which minimizes the structural deformation prior to the Coulomb explosion.

In conclusion, we have demonstrated that the Coulomb explosion dynamics of H_2S in intense laser fields can be manipulated by the polarization direction ε in the molecular frame. The observed dependence of the electronic and nuclear responses to the non-resonant laser fields can be explained in terms of the character of the CT states, which serve as the "doorway states" to the structural deformation of small polyatomic molecules in intense laser fields as well as to the ionization and fragmentation processes discussed previously. The understanding of the electronic and nuclear response to the laser fields polarized in the molecular frame presented here will provide new prospects for efficient quantum control in the intense field regime.

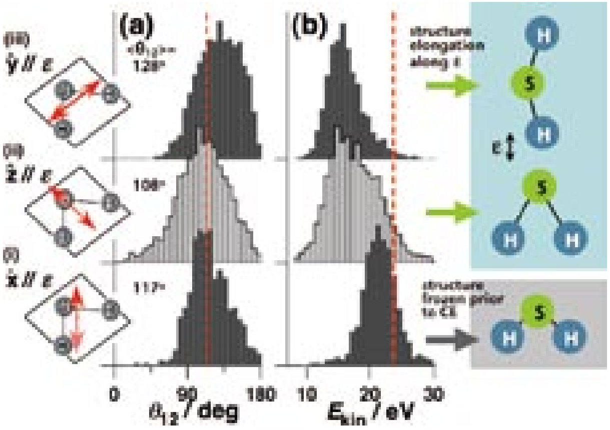

Figure 1. (a) Momentum angle θ_{12} distribution and (b) total kinetic energy E_{kin} distribution obtained for three different directions of ε, in the molecular frame, (i) $x//\varepsilon$, (ii) $y//\varepsilon$ and (iii) $z//\varepsilon$.

2. Dalitz Plot Analysis of Coulomb Exploding O_3 in Ultrashort Intense Laser Fields[2)]

The three-body Coulomb explosion of ozone, $O_3^{3+} \rightarrow O^+ + O^+ + O^+$, in ultrashort intense laser fields (2×10^{15} W/cm^2) is studied with two different pulse durations (9 and 40 fs) by the coincidence momentum imaging method. The nuclear dynamics in the laser fields is discussed using the Dalitz plot,[3)] developed originally to describe the three-body reactions in elementary particle physics, which provides a compact two-dimensional representation of the relative momentum sharing among the three fragments produced through the dissociation of small polyatomic molecules.

In a Dalitz plot, normalized kinetic energy parameters of the three fragments are plotted in the Cartesian coordinate system (x,y),

$$x = (\varepsilon_1 - \varepsilon_2)/(\sqrt{3}E_{kin}), \qquad (1)$$
$$y = \varepsilon_3/E_{kin} - 1/3, \qquad (2)$$

where ε_i is the kinetic energy of the i-th fragment and $E_{kin} = \varepsilon_1 + \varepsilon_2 + \varepsilon_3$. A set of three fragment momenta that fulfills the momentum conservation condition falls within a circle of 1/3 in radius in this plot, and form a uniform distribution if there is no correlation among the three fragment momenta.

The Dalitz plot obtained for the 9-fs intense laser fields exhibits a sharp peak centered at the origin as shown in Figure 2, showing that all the three fragment ions tend to have the same momentum values, by the strong Coulombic interactions during the explosion process. When the pulse duration is increased from 9 to 40 fs, a broadening of the Dalitz plot distribution is identified, in addition to a decrease in the total kinetic energy release. The analysis based on a simple Coulomb explosion model shows that the geometrical structure of ozone remains almost unchanged during the interaction with the few-cycle intense laser fields, while a significant structural deformation along all the three vibrational coordinates, including the anti-symmetric stretching coordinate, is identified in the 40 fs laser fields. The observed nuclear dynamics are discussed in terms of the population transfer to the excited states of O_3.

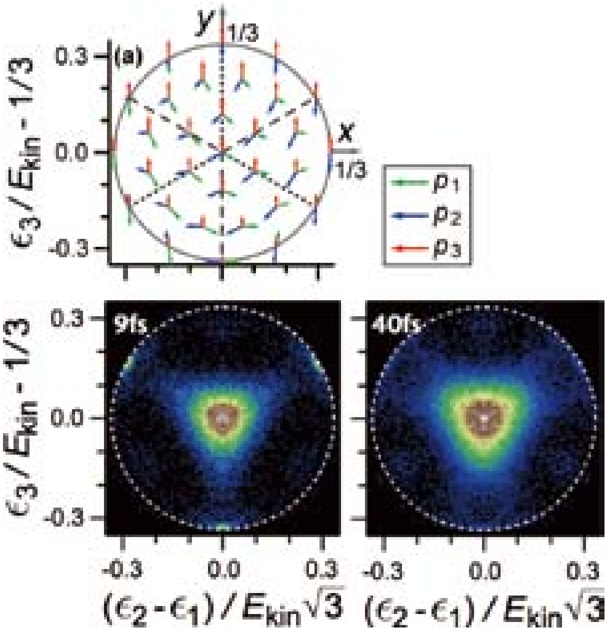

Figure 2. Dalitz plots obtained for the Coulomb explosion process of ozone, $O_3^{3+} \rightarrow O^+ + O^+ + O^+$, in 9 and 40 fs intense laser fields (2×10^{15} W/cm^2).

References

1) A. Hishikawa. E. J. Takahashi and A. Matsuda, *Phys. Rev. Lett*. **96**, 243002 (2006).
2) A. Matsuda, E. J. Takahashi and A. Hishikawa, *J. Chem. Phys*. **127**, 114318 (2007).
3) R. H. Dalitz, *Philos. Mag*. **44**, 1068–1080 (1953).

Award

HISHIKAWA, Akiyoshi; Morino Fundation for Molecular Science.

Light Source Developments by Using Relativistic Electron Beams

UVSOR Facility
Division of Advanced Accelerator Research

KATOH, Masahiro	Professor
HOSAKA, Masahito	Assistant Professor*
MOCHIHASHI, Akira	Assistant Professor
SHIMADA, Miho	IMS Fellow
KOIKE, Masashi	Graduate Student†
SUZUKI, Yasuhiro	Graduate Student†
YOSHIDA, Mitsuhiro	Graduate Student†

This project involves researches and developments on synchrotron light source, accelerator technologies, beam physics, free electron laser and related technologies. All these works are performed at UVSOR-II electron storage ring and its injector.

1. Developments on UVSOR-II Accelerators

After the major upgrade in 2003,[1] the UVSOR-II electron storage ring and its injector has been continuously improved. In this year an undulator was constructed and installed as the fourth undulator in the facility (Figure 1). The magnetic configuration is so-called APPLE-II type. The undulator can provide VUV light of various polarizations (horizontal /vertical plane and right-/left-handed circular) to a beam-line dedicated for photo-electron spectroscopy.[2] Its main parameters are summarized in Table 1. The commissioning was successful. The electron orbit movement caused by the magnetic field changes could be suppressed to smaller than 10 microns by a feed-forward system.

Figure 1. New variable polarization undulator for BL7U.

Table 1. Parameters of New Variable Polarization Undulator.

Configuration	APPLE-II	
Number of Periods	40	
Period Length	76 mm	
Pole Length	3.04 m	
Pole Gap	24–200 mm	
Max. K Parameter	5.4	(horizontal)
	3.6	(vertical)
	3.0	(helical)

The beam lifetime of UVSOR-II is severely limited by Touschek effect due to its low emittance and low electron energy. The electron beam should be re-filled every 6 hours. To solve the lifetime problem eternally, we are preparing for top-up injection scheme. In this scheme, the electron beam is re-filled with a short interval, typically one minutes, to keep the beam current almost constant.

Figure 2. New magnet power supply for the booster synchrotron.

To realize the top up injection, the maximum operating energy of the injector and the beam transport line had to be increased from 600 MeV to 750 MeV. In this year, the magnet power supplies of the booster synchrotron and the beam transport line were replaced. The new power supplies are capable of exciting the existing magnets sufficiently strong for the 750 MeV operation. The new power supplies were successfully commissioned. Soon, we have succeeded in accelerating electrons up to 750 MeV on the booster synchrotron and also in transporting those electrons to the storage ring. In July, we have started the full energy injection in the user runs. After some improvements on the beam transport efficiency and reinforcements on the beam monitor system and the safety interlock system, we will start testing the top-up injection soon.

2. New Method to Measure Touschek Lifetime

Touschek effect is a dominant beam loss mechanism in a low emittance and low energy storage ring such as UVSOR-II. It is difficult to measure the beam loss rate due to Touschek effect separately from those due to other effects such as scattering by residual gas molecules. We have developed a new method to measure the Touschek lifetime separately from other process.3) The method is based on the single photon counting technique. By measuring the change of the relative intensities of two successive bunches, we can estimate the Touschek lifetime independently.

3. Storage Ring Free Electron Laser

The low emittance and the high peak current of UVSOR-II make the free electron laser oscillate in the deep UV region with high output power exceeding 1W.4) At present the shortest wavelength is 215 nm. Lasing around 200 nm seems promising. Users' experiments using this high power and tunable laser beam are in progress.5)

The interaction between the electron beam and the laser pulse in the optical cavity produce strong electron bunch heating. This process limits the output power of the free electron laser. This heating process and its effects on the lasing were experimentally investigated.6)

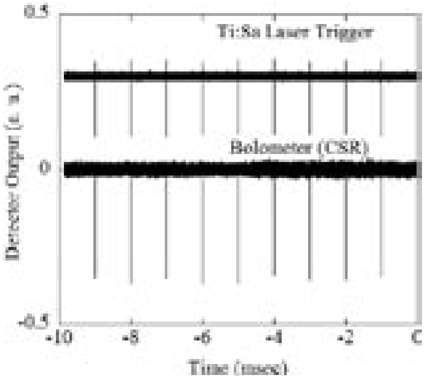

Figure 3. Coherent terahertz radiation induced by laser injection.

4. Terahertz Coherent Synchrotron Radiation by Laser-Electron Interaction

We have developed a system to create micro-density structure on electron bunches circulating in the storage ring.7) The density structure, whose typical scale is ranging from a few hundred femtoseconds to a few picoseconds, is created through the interaction between the ultra-short laser pulses and electron bunches. Such electron bunches emit coherent synchrotron radiation in terahertz region, as shown in Figure 3. It was successfully demonstrated that, by controlling the shape of the micro-structure, the spectra of the coherent radiation could be controlled.

5. Coherent Harmonic Generation

Coherent harmonic generation is a method to produce coherent harmonics of laser light by using relativistic electron beam. The laser-electron interaction in an undulator produces density modulation of a period of laser wavelength. When the energy modulation is sufficiently larger than the natural energy spread, the density modulation contains higher harmonic component of the laser wavelength. Such an electron bunch emits coherent harmonics of the injected laser. We have successfully observed the coherent third harmonics of Ti:Sa laser.8) Optical properties of the coherent harmonic radiation were experimentally investigated.

References

1) M. Katoh, M. Hosaka, A. Mochihashi, J. Yamazaki, K. Hayashi, Y. Hori, T. Honda, K. Haga, Y. Takashima, T. Koseki, S. Koda, H. Kitamura, T. Hara and T. Tanaka, *AIP Conf. Proc*. **705**, 49–52 (2004).

2) S. Kimura, T. Ito, E. Nakamura, M. Hosaka and M. Katoh, *AIP Conf. Proc.* **879**, 527–530 (2007).

3) A. Mochihashi, M. Katoh, M. Hosaka, Y. Takashima and Y. Hori, *Nucl. Instrum. Methods Phys. Res., Sect. A* **572**, 1033–1041 (2007).

4) M. Hosaka, M. Katoh, A. Mochihashi, M. Shimada, T. Hara and Y. Takashima, *Proc. 28th Internat. Free Electron Laser Conf.* (2006, Berlin), 368–370 (2006).

5) *e.g.* T. Nakagawa, T. Yokoyama, M. Hosaka and M. Katoh, *Rev. Sci. Instrum.* **78**, 023907 (2007).

6) M. Labat, M. E. Couprie, M. Hosaka, A. Mochihashi, M. Katoh and Y. Takashima, *Phys. Rev. STAB* **9**, 100701 (2006).

7) M. Katoh, M. Hosaka, A. Mochihashi, M. Shimada, S. Kimura, Y. Takashima and T. Takahashi, *AIP Conf. Proc*. **879**, 71–73 (2007).

8) M. Labat, M. Hosaka, A. Mochihashi, M. Shimada, M. Katoh, G. Lambert, T. Hara, Y. Takashima and M. E. Couprie, *Eur. Phys. J. D* **44**, 187–200, e2007-00177-6 (2007).

---

* Present address; Nagoya University, Nagoya, 464-8603

† carrying out graduate research on Cooperative Education Program of IMS with other graduate schools

Synchrotron Radiation Spectroscopy on Strongly Correlated Electron Systems

UVSOR Facility
Division of Advanced Solid State Physics

KIMURA, Shin-ichi	Associate Professor
ITO, Takahiro	Assistant Professor
SAKURAI, Yoko	IMS Fellow*
IM, Hojun	Post-Doctoral Fellow†
SUMII, Ryohei	Post-Doctoral Fellow‡
MIZUNO, Takafumi	Graduate Student
MIYAZAKI, Hidetoshi	Graduate Student§
OTA, Syunji	Graduate Student§,‖
MIZUNUMA, Takuro	Graduate Student¶,**
IIZUKA, Takuya	Graduate Student††

Solids with strong electron–electron interaction, so-called strongly correlated electron systems (SCES), have various physical properties such as non-BCS superconducting, colossal magneto-resistance, heavy fermion and so on. The materials are one of candidates of the next generation functional materials. We are investigating the mechanism of the physical properties of SCES, especially rare-earth compounds, organic superconductors and transition-metal compounds, by infrared and angle-resolved photoemission spectroscopies using synchrotron radiation. Since experimental techniques using synchrotron radiation are evolved rapidly, the development is also one of our research subjects.

1. Optical Observation of Non-Fermi-Liquid Behavior in the Heavy Fermion State of YbRh$_2$Si$_2$1)

The crossover between the localized and itinerant properties of rare-earth compounds is one of the main topics of recent solid state physics. We investigate the change of the electronic structure from the localized to itinerant states *via* the quantum critical point. The control from the localized to itinerant properties is usually done by applying pressure or changing the concentration of ligand atoms. YbRh$_2$Si$_2$ is a recently developed non-Fermi liquid material and is located near the quantum critical point. At the quantum critical point, the electrical resistivity is proportional to the temperature ($\rho \propto T$) below 10 K that is different from the Femi liquid property ($\rho \propto T^2$). Then we measured far-infrared optical properties of YbRh$_2$Si$_2$ for photon energies down to 2 meV and temperatures 0.4–300 K. In the coherent heavy quasiparticle state, a linear dependence of the low-energy scattering rate on both temperature and photon energy was found (Figure 1). We relate this distinct dynamical behavior different from that of Fermi-liquid materials to the non-Fermi-liquid nature, *i.e.*, the electrodynamic property of YbRh$_2$Si$_2$ also indicates the non-Fermi liquid nature.

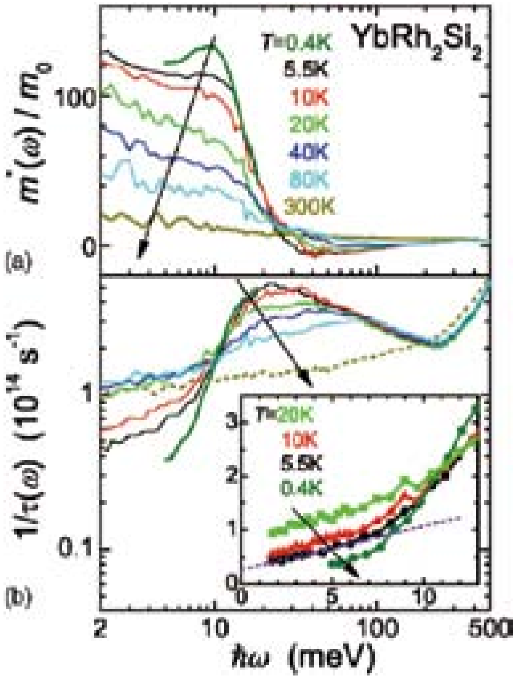

Figure 1. Temperature dependence of (a) the effective mass relative to the free-electron mass, $m^*(\omega)/m_0$, and (b) the scattering rate $1/\tau(\omega)$ as a function of photon energy. The inset of (b) is the low-energy part of $1/\tau(\omega)$. The dashed line emphasizes a $1/\tau(\omega) \propto \omega$ behavior.

2. Magnetic-Field-Induced Superconductor–Insulator–Metal Transition in an Organic Conductor: An Infrared Magneto-Optical Imaging Spectroscopic Study2)

The magnetic-field-induced superconductor–insulator–metal transition (SIMT) in partially deuterated κ-(BEDT-TTF)$_2$Cu[N(CN)$_2$]Br, which is just on the Mott boundary, has been observed using the infrared magneto-optical imaging spectroscopy. The infrared reflectivity image on the sample surface revealed that the metallic (or superconducting) and insulating phases coexist and they have different magnetic-field dependences as shown in Figure 2. One of the magnetic-field dependence is SIMT that appeared on part of the sample surface. The SIMT was concluded to originate from the balance of the inhomogeneity in the sample itself and the disorder of the ethylene end groups resulting from fast cooling.

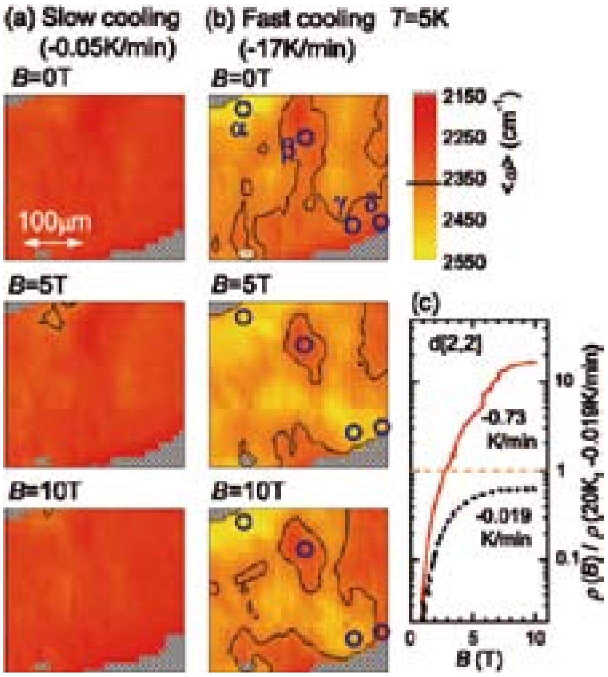

Figure 2. Magnetic-field and cooling-rate [slow cooling in (a) and fast cooling in (b)] dependencies of the spatial image of the center of the spectral weight <ω> of 50% deuterated κ-(BEDT-TTF)$_2$Cu[N(CN)$_2$]Br (*d*[2,2]) at T = 5 K. The wavenumber of <ω> below (above) 2350 cm^{-1} is metallic (insulating) region. The black lines indicate the rough *M*–*I* boundary (ω_{MI}) of 2350 cm^{-1} and the lower and higher wave numbers indicate the insulating and metallic (superconducting) reflectivity spectra, respectively. The blue circles in (b) indicate the points of the different magnetic-field dependences on the sample surface. The hatched area is the outside of the sample. (c) Magnetic-field and cooling-rate dependencies of the normalized resistivity of *d*[2,2] at 5.5 K for the reference. Though the cooling rate of –0.73 K/min is different from that of (b), the physical character is the same.

3. Infrared Reflection-Absorption Spectroscopy of Alq$_3$ Thin Film on Silver Surface Using Synchrotron Radiation[3)]

Infrared reflection-absorption spectra of Alq$_3$ film on Ag surface have been measured as a function of thickness in the wave number region from 300 to 500 cm^{-1} using synchrotron radiation, UVSOR-II, to determine which of the geometrical isomers of Alq$_3$ is dominant. The observed spectra of the Al–N stretching modes of Alq$_3$ at around 420 cm^{-1} indicate that Alq$_3$ film predominantly consists of the meridional isomer including the first monolayer adsorbed on the Ag surface as shown in Figure 3. In the spectrum of the monolayer Alq$_3$, the Al–N stretching mode was observed to be located at wave number slightly lower than that of multilayer Alq$_3$ probably due to the charge transfer between Alq$_3$ and the Ag surface.

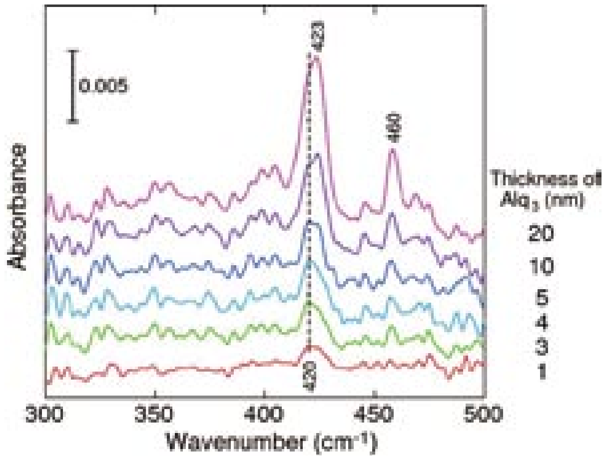

Figure 3. The thickness dependence of the IRAS spectra of an Alq$_3$ film on Ag surface.

References

1) S. Kimura, J. Sichelschmidt, J. Ferstl, C. Krellner, C. Geibel and F. Steglich, *Phys. Rev. B* **74**, 132408 (4 pages) (2006).
2) T. Nishi, S. Kimura, T. Takahashi, H. J. Im, Y. S. Kwon, T. Ito, K. Miyagawa, H. Taniguchi, A. Kawamoto and K. Kanoda, *Phys. Rev. B* **75**, 014525 (5 pages) (2007).
3) Y. Sakurai, S. Kimura and K. Seki, *Appl. Phys. Lett.* **91**, 061922 (3 pages) (2007).

---

* Present Address; JAEA/SPring-8, Sayo, Hyogo 679-5148

† from Sungkyunkwan University, Korea

‡ from Nagoya University

§ carrying out graduate research on Cooperative Education Program of IMS with Nagoya University

|| Present Address; INAX Co. Ltd.

¶ carrying out graduate research on Cooperative Education Program of IMS with Meiji University

** Present Address; Department of Physics, Meiji University, Kawasaki 214-8571

†† carrying out graduate research on Cooperative Education Program of IMS with Kobe University

Electronic Structure and Decay Dynamics in Atoms and Molecules Following Core Hole Creation

UVSOR Facility
Division of Advanced Photochemistry

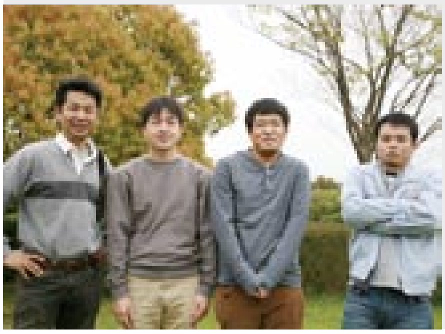

SHIGEMASA, Eiji	Associate Professor
HIKOSAKA, Yasumasa	Assistant Professor
KANEYASU, Tatsuo	IMS Fellow
ITOH, Masahiro	Graduate Student*

The dynamics of the inner-shell photoexcitation, photoionization, and subsequent decay processes is much more complex, in comparison to outer-shell photo-processes. For instance, the inner-shell photoionization is concomitant with the excitation and ionization of valence electrons, which reveal themselves as shake-up and shake-off satellite structures in the corresponding photoelectron spectrum. The one-photon multi-electron processes, which are entirely due to the electron correlation in the system, are known to happen not only in the primary inner-shell hole creation processes, but also in their relaxation processes. Our research project is focused on elucidating the electronic structures and decay dynamics in core-excited atoms and molecules, by utilizing various spectroscopic techniques together with monochromatized synchrotron radiation in the soft x-ray region.

1. Dissociation Dynamics in Polyatomic Molecules Following Core Hole Creation

Auger electron-ion coincidence is a powerful method for studying the decay dynamics of core-excited/ionized molecules produced by soft x-ray irradiation. In order to exert the full potential of this method, the spectrometer should be equipped with a performance realizing analyses of vector correlations among the momenta of all the particles emitted. Coincidence imaging spectrometers, which enable us to measure three-dimensional momenta of both the electron and ions, have been widely used in the research field of atomic and molecular science. However it is difficult for such imaging technique to observe fast Auger electrons with a sufficient energy resolution. In this respect, a conventional electrostatic analyzer is suitable for observing the fast Auger electrons.

We have newly developed an Auger electron-ion coincidence spectrometer which consists of a double toroidal electron analyzer and a three-dimensional ion momentum spectrometer.[1)] The performance has been evaluated by measuring Auger electrons and photoions emitted after inner-shell photoionization of OCS.

2. One-Photon Multi-Electron Emission Processes Studied by Multi-Eelectron Coincidence Spectroscopy

The double photoionization (DPI) of atoms and molecules has attracted special attention for a long time because this process is due entirely to electron correlation and, consequently, investigations of DPI reveal fundamental aspects of atomic and molecular physics. Until now, most DPI studies have concentrated on the removal of two valence electrons. Direct experimental observations of core-valence or core-core DPI are limited to a few cases. This is because investigations using conventional photoelectron spectroscopy offer neither direct spectroscopy of the doubly-ionized states nor the detailed DPI dynamics. By contrast, coincidence detection between the two photoelectrons emitted in DPI processes provides direct spectroscopic information on DPI processes; however, a sophisticated coincidence method is required, because the DPI cross section is unfavorable as compared with the main inner-shell ionization processes and, consequently, the events associated with these DPI processes are easily hidden behind ordinary inner-shell photoionization events. We have introduced a very efficient coincidence technique, the magnetic bottle time-of-flight electron coincidence method, into an investigation of DPI associated with the removal of a core electron. The powerful capabilities of this coincidence method on electron coincidence observations have recently been described.[2–5)]

A multi-electron coincidence dataset for Xe was accumulated at a photon energy of 301.6 eV.[6)] Figure 1(a) shows the photoelectron spectrum in the kinetic energy range of 60–

250 eV, and Figure 1(b) displays a two-dimensional (2D) map showing coincidences between photoelectrons and slower electrons in the energy range 0–100 eV. Several diagonal stripes are observed on the 2D map. They are due to coincidences between two photoelectrons emitted through core-core or core-valence DPI. The intensity distributions along the diagonal stripes describe how the two photoelectrons produced from the DPI processes share the available energy. Resonance structures are discernable on the distributions: interactions and interference of the Xe^+ states with the DPI continua can be discussed from the resonance features.

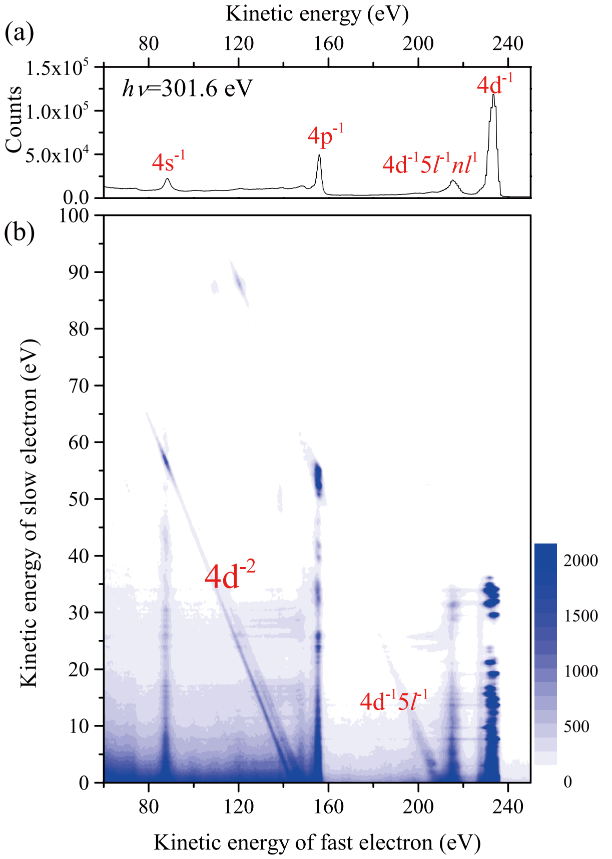

Figure 1. (a) Photoelectron spectrum of Xe obtained at a photon energy of 301.6 eV. (b) Two dimensional map of all coincidence pairs, represented as a function of the kinetic energies of fast and slow electrons.

3. Electronic Structures and Decay Dynamics in Multiply Excited States of Simple Molecules

Excitation of a core-electron in molecules can be accompanied by promotion of one or several valence electrons, due to the electron relaxation (valence polarization) and correlation effect. Such core-valence doubly or multiply excited states usually lie above the corresponding core ionization thresholds. The doubly excited states of N_2 are exhibited on the photoabsorption spectrum in the photon energy range of 413–416 eV. We have performed an inner-shell photoelectron spectroscopic study of the autoionization of the core-valence doubly excited states.[7] The principal concern is the interplay between the autoionization from the doubly excited states and the femtosecond nuclear motion. The vibrational structure of the $N_2^+(1\sigma_{g/u}^{-1})$ states in photoelectron spectra manifests the relative rates for autoionization and nuclear motion.

In order to investigate all the autoionization features of the doubly excited states, we measured photoelectron spectra in the region of 412.5–417.3 eV with the photon energy intervals of 50 meV, at both 0° and 90° with respect to the electric vector. For an effective presentation of the obtained photoelectron spectra, 2D maps were used (Figures 2 (a) and (b)). The 2D maps show clearly that the vibrational features of the $N_2^+(1\sigma_{g/u}^{-1})$ states depends strongly on both photon energy and detection angle.

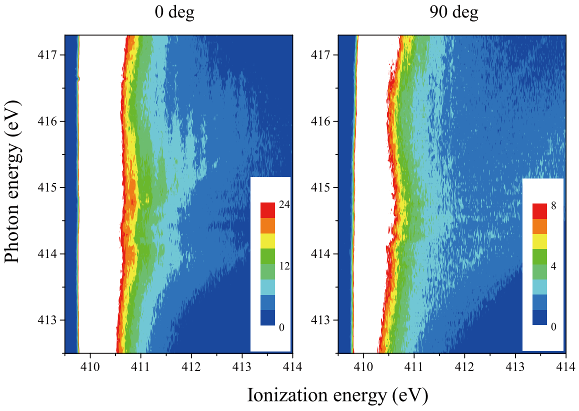

Figure 2. Two-dimensional maps of the inner-shell photoelectron yields from N_2 as a function of photon energy and ionization energy, measured in the photon energy region of 412.5–417.3 eV at (a) 0° and (b) 90° with respect to the electric vector.

References

1) T. Kaneyasu, Y. Hikosaka and E. Shigemasa, *J. Electron. Spectrosc. Relat. Phenom.* **156-158**, 279–283 (2007).
2) Y. Hikosaka, T. Aoto, P. Lablanquie, F. Penent, E. Shigemasa and K. Ito, *Phys. Rev. Lett.* **97**, 053003 (4 pages) (2006).
3) Y. Hikosaka, T. Aoto, P. Lablanquie, F. Penent, E. Shigemasa and K. Ito, *J. Phys. B* **39**, 3457–3464 (2006).
4) T. Kaneyasu, Y. Hikosaka, E. Shigemasa, F. Penent, P. Lablanquie, T. Aoto and K. Ito, *Phys. Rev. A* **76**, 012717 (7 pages) (2007).
5) Y. Hikosaka, T. Kaneyasu, E. Shigemasa, P. Lablanquie, F. Penent and K. Ito, *J. Chem. Phys.* **127**, 044305 (2007).
6) Y. Hikosaka, P. Lablanquie, F. Penent, T. Kaneyasu, E. Shigemasa, J. H. D. Eland, T. Aoto and K. Ito, *Phys. Rev. Lett.* **98**, 183002 (4 pages) (2007).
7) Y. Hikosaka, T. Kaneyasu, E. Shigemasa, Y. Tamenori and N. Kosugi, *Phys. Rev. A* **75**, 042708 (5 pages) (2007).

* carrying out graduate research on Cooperative Education Program of IMS with Niigata University

Micro Solid-State Photonics

Laser Research Center for Molecular Science
Division of Advanced Laser Development

TAIRA, Takunori	Associate Professor
ISHIZUKI, Hideki	Assistant Professor
AKIYAMA, Jun	IMS Fellow
TSUNEKANE, Masaki	Post-Doctoral Fellow*
SATO, Yoichi	Post-Doctoral Fellow
SAIKAWA, Jiro	Post-Doctoral Fellow†
OISHI, Yu	Post-Doctoral Fellow‡
ONO, Yoko	Secretary
INAGAKI, Yayoi	Secretary

The artistic optical devices should be compact, reliable, efficient and high power light sources. With the approaches of domain structures and boundaries engineering, it is possible to bring the new interaction in their coherent radiation. The high-brightness nature of Yb or Nd doped single crystal or ceramic microchip lasers can realize efficient nonlinear wavelength conversion. In addition, designed nonlinear polarization under coherent length level allows us new function, such as the quasi phase matching (QPM). The development of "***Micro Solid-State Photonics***," which is based on the micro domain structure and boundary controlled materials, opens new horizon in the laser science.

1. High-Power Operation of Diode Edge-Pumped, Composite All-Ceramic Yb: $Y_3Al_5O_{12}$ Microchip Laser

A solid-state laser material of composite all-ceramic Yb: $Y_3Al_5O_{12}$ is applied as a source of a high-power, diode edge-pumped microchip laser. 520 W quasi-continuous-wave and 414 W continuous-wave (cw) output powers were obtained from the 3.7-mm-diameter, Yb doped ceramic core with a 200 µm thickness. The cw output power densities of 3.9 kW/cm^2 and 0.19 MW/cm^3 in the core area and volume, respectively, are the highest for an active-mirror solid-state laser. The maximum thermal stress in the ceramic core is estimated to be 384 MPa at the non-cooled surface and is twice the tensile strength of single-crystal $Y_3Al_5O_{12}$. Figure 1 shows the input and output laser characteristics in quasi-cw (10 ms, 10 Hz) and cw operations of the composite all-ceramic Yb:YAG EPMCL.

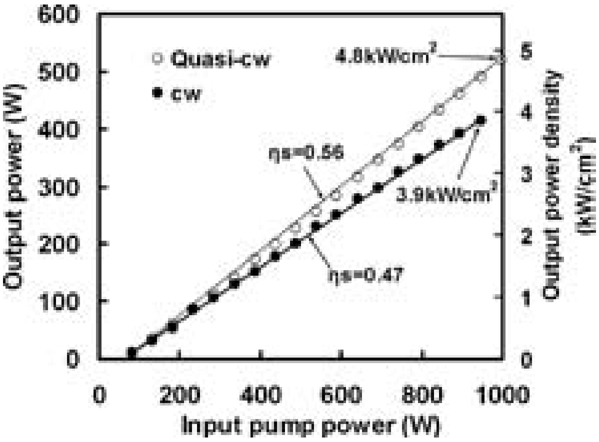

Figure 1. Incident pump power (peak) *vs.* laser output power (peak) of the edge-pumped all-ceramic EPMCL in quasi-cw and cw operations. The right axis shows output power density from the core area.

2. The Studies of Thermal Conductivity in $GdVO_4$, YVO_4, and $Y_3Al_5O_{12}$ Measured by Quasi-One-Dimensional Flash Method

We have measured thermal conductivity of $Y_3Al_5O_{12}$, $GdVO_4$, and YVO_4. In order to avoid the miss leading from three-dimensional (3D) thermal diffusion, we developed the quasi-one-dimensional (q1D) flash method. By taking in account the heat radiation effect in transparent materials for this measurement, YVO_4 was found to have larger thermal conductivity than $GdVO_4$. The measured thermal conductivities were 12.1, 10.5, 10.1, 8.9, and 8.5 W/mK for *c*-cut YVO_4, *c*-cut $GdVO_4$, YAG, *a*-cut YVO_4, and *a*-cut $GdVO_4$, respectively. The measured value in the range from room temperature to 200 °C is shown in Figure 2. The dependence of Nd-conductivity coefficient ($d\kappa/dC_{Nd}$) for convenient evaluation of the doping effect in thermal conductivity is also discussed.

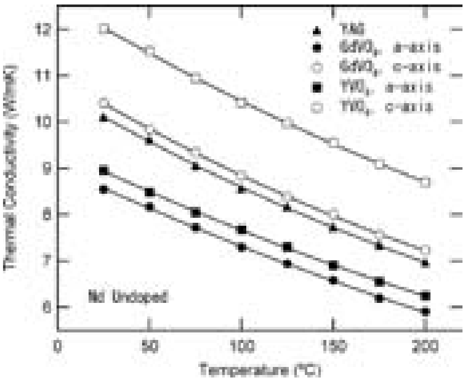

Figure 2. The measured value in the range from room temperature to 200 °C.

3. 52mJ Narrow-Bandwidth Degenerated Optical Parametric System with a Large-Aperture Periodically Poled MgO:LiNbO$_3$ Device

We have demonstrated efficient, high-energy, narrow-spectral-bandwidth 2.128µm pulse generation by use of periodically poled MgO:LiNbO$_3$ devices with a 36 mm length and 5 mm × 5 mm large aperture. A free-running degenerated optical parametric oscillator (OPO) pumped with a Q-switched 1.064µm Nd:YAG laser exhibits a high slope efficiency of 75% and an optical-to-optical conversion efficiency of 70% with a broad spectral bandwidth (> 100 nm). In a configuration with a spectrally narrowed master oscillator followed by a power amplifier, we have achieved an output pulse energy of 52 mJ with a spectral bandwidth of less than 2 nm at the degeneracy point. The total optical-to-optical conversion efficiency of the system reached 50%.

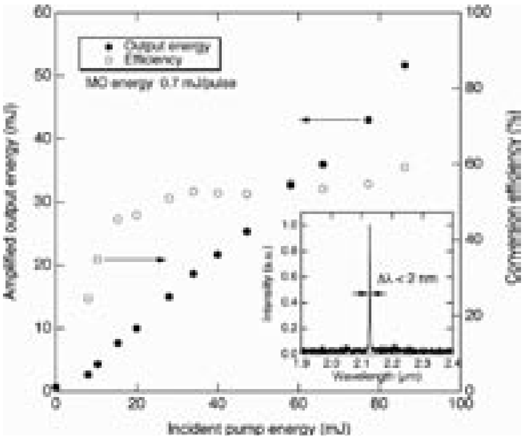

Figure 3. OPA output energy and conversion efficiency versus incident pump energy. The MO energy was 0.7 mJ/pulse. Closed circles, amplified pulse energy; open circles, conversion efficiency.

4. Tailored Spectral Designing of Layer-by-Layer Type Composite Nd:Y$_3$ScAl$_4$O$_{12}$/Nd:Y$_3$Al$_5$O$_{12}$ ceramics

We have fabricated the all-ceramic layered composite device with Nd:YAG and Nd:YSAG, which can perform efficient laser oscillation. From its spectroscopic properties, this layer-by-layer composite device will offer new function of laser oscillation by pump wavelength tuning. For example when pumped from YSAG side at 810.5 nm, it can oscillate at 1064 nm. On the other hand, it will oscillate at 1061 nm when pumped at 808.5 nm.

Due to the difference in the dependence on the wavelength of, the portion of the pumped power absorbed in Nd:YAG-layer and in Nd:YSAG-layer depends on the pumping wavelength. This resulted in the tuning of the component ratio of the Nd:YAG and Nd:YSAG in the fluorescence. The dependence of fluorescence profiles in this composite on the pump wavelength is shown in Figure. 4.

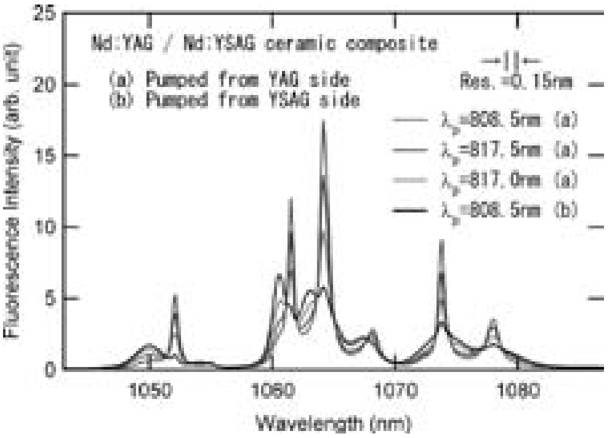

Figure 4. Measured fluorescent spectral profiles by changing pumping wavelength.

References

1) M. Tsunekane and T. Taira, *Appl. Phys. Lett.* **90**, 121101 (3 pages) (2007).
2) Y. Sato and T. Taira, *Opt. Express* **14**, 10528–10536 (2006).
3) J. Saikawa, M. Fujii, H. Ishizuki and T. Taira, *Opt. Lett.* **31**, 3149–3151 (2006).
4) Y. Sato, A. Ikesue and T. Taira, *IEEE J. Sel. Top. Quantum Electron.* **13**, 838–843 (2007).

---

* from JST Innovation Plaza Tokai
† from Tokyo Institute of Technology
‡ from RIKEN

Photo-Induced Dynamics and Reactions at Solid Surfaces

Laser Research Center for Molecular Science
Division of Ultrahigh Resolution Optical Measurement

MATSUMOTO, Yoshiyasu Professor
WATANABE, Kazuya Assistant Professor
MATSUMOTO, Taketoshi Assistant Professor*
NAKAI, Ikuyo Post-Doctoral Fellow†
FUYUKI, Masanori Graduate Student‡

Solid surfaces provide an interesting environment where two completely different electronic systems meet to each other: localized electronic system, *i.e.*, atoms and molecules and delocalized one, *i.e.*, solid bulk surfaces. Charge transfer at surfaces is fundamental to adsorbate-metal interactions and reactions. Moreover, dynamic processes including chemical reactions on surfaces, particularly metal surfaces, are associated with continuous nonadiabatic transitions. This research program aims for understanding electron and nuclear dynamics at surfaces. Photo-induced processes including photochemistry at surfaces are the major focus in this program. Photons are used for not only exciting electronic states of adsorbate and substrate, but also for probing those states with various types of nonlinear optical spectroscopy.

1. Ultrafast Dynamics at Well-Defined Surfaces[1–3]

To understand the mechanism of surface photochemistry, it is vital to know how photoinduced electronic excitation induces adsorbate nuclear motions that ultimately lead to chemical reactions. We have demonstrated the real-time observations of surface phonons and adsorbate-substrate vibrational modes by fs time-resolved second harmonics generation (TRSHG). If an excitation light pulse has a duration sufficiently shorter than a period of a vibrational mode or a phonon mode, it can excite the mode with a high degree of temporal and spatial coherence. This coherent nuclear motion modulates the second-order susceptibility $\chi^{(2)}$. Thus, by monitoring the intensity modulation of the second harmonics (SH) generation of a probe pulse, we can observe the evolution of the coherent nuclear motion subsequent to the electronic excitation at the surfaces. We have focused on K on Pt(111), and Na and K on Cu(111) adsorption systems.

We have investigated coherently excited surface phonons at K-covered Pt(111) surfaces by using femtosecond time-resolved second harmonic generation spectroscopy. The frequency of the K–Pt stretching phonon mode depends on the superstructure of K: 5.0–5.3 and 4.5–4.8 THz for (2×2) and ($\sqrt{3}\times\sqrt{3}$)R30° superstructures, respectively. In addition to the stretching mode, a couple of Pt surface phonon modes are simultaneously observed when the ($\sqrt{3}\times\sqrt{3}$)R30° superstructure is formed. The dephasing time of the K–Pt stretching mode becomes shorter and its frequency redshifts as the absorbed fluence of a pump pulse increases. This is in stark contrast to the Pt surface phonon modes whose frequencies are independent of fluence. The fluence dependence of the K–Pt stretching mode is interpreted to be due to anharmonic coupling between the K–Pt stretching and lateral modes.

We have also observed time-resolved second harmonic signals from the Cu(111) surface with a full monolayer of Na in ultra-high vacuum and investigated the excitation-wavelength dependence of the wave packet dynamics of the coherently excited Na–Cu stretching mode. Changing the photon energy of the pump pulse (25 fs) from 2.0 to 2.5 eV, the oscillation amplitude derived from the Na–Cu stretching motion is enhanced. The careful measurements of photon-energy dependence indicates that the excitation efficiency mimics the absorbance of bulk Cu. Holes created in the d-bands by the optical transitions could be filled by electrons in the adsorbate-induced occupied state of the metallic quantum well by an Auger-type transition. Hence, holes can be created in the adsorbate-induced occupied state. Moreover, since this Auger decay can occur significantly faster than the oscillation period of the Na–Cu stretching mode, the substrate excitation may be a possible excitation mechanism for the coherent oscillation.

2. Spectroscopy and Chemistry of Metal Nanoclusters on Surfaces[4)]

The structure and reactivity of metal nanoclusters are important issues because of their relevance to heterogeneous catalysis. In particular, Au nanoclusters on titanium oxide surfaces has attracted a lot of interest since the discovery of its catalytic activity on CO oxidation. We apply various surface science techniques to clarify correlations between structures and reactivity of metal nanoclusters deposited on surfaces. We use alkanethiolate-coated gold nanoclusters as a primary target in collaboration with Tsukuda (IMS) and Al-Shamery (U. Oldenburg) groups.

Deposition and fabrication of films of Au nanoclusters protected by alkanethiolate ligands are attempted on a TiO_2 (110) surface and the structures of films are observed by a scanning tunneling microscope (STM). Effects of oxygen- and hydrogen-plasma etching in addition to UV irradiation on the structure and chemical composition of the films are also investigated by using STM and X-ray photoelectron spectroscopy. Alkanethiolate Au nanoclusters are produced using a modified Brust synthesis method and their LB films are dip-coated on TiO_2(110). Alkanethiolate Au nanoclusters are weakly bound to the substrate and can be manipulated with an STM tip. Net-like structures of alkanethiolate Au nanoclusters are formed by a strong blast of air. Oxygen plasma etching removes alkanethiolate ligands and simultaneously oxidizes Au clusters. At room temperature, prolonged oxygen plasma etching causes agglomeration of Au nanoclusters. UV irradiation removes ligands partly, which makes Au nanoclusters less mobile. The net-like structure of alkanethiolate Au clusters produced by a blast of air is retained after oxygen- and hydrogen-plasma etching.

3. Observation of Spatial Patterning by a Sum Frequency Generation Microscope

For understanding of heterogeneous reactions on solid surfaces, it is crucial to obtain how reactions evolve in time and spatial domains. For this purpose, a new microscope for observation of spatial patterning of reactants and products at surfaces is needed. It is highly desirable that the microscope is capable to identify chemical species.

Sum frequency generation (SFG) is a nonlinear optical process. In particular, when visible and infrared beams are used, SFG is a powerful means for vibrational spectroscopy. Thus, we are developing a SFG microscope. So far, the first prototype of a microscope (Figure 1) has been built and micropatterns of self-assembled monolayer have been observed. The spatial resolution of the current microscope is about 5 µm.

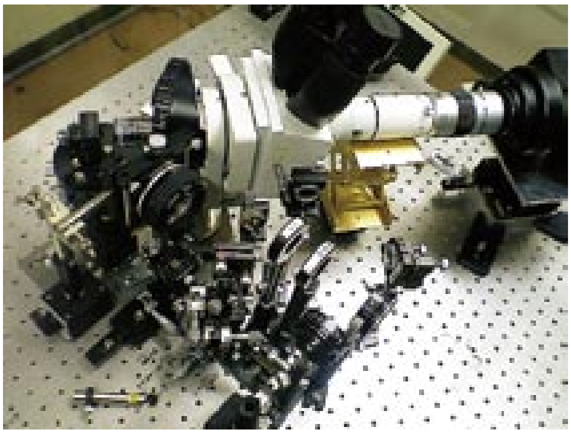

Figure 1. Setup of the sum frequency generation microscope.

4. Chemistry of One-Dimensional Nano-Surface Compounds

The fluctuating configurations of low-dimensional structures can be thermodynamically favorable at finite temperatures, because the energy gain overcomes the energy cost that accompanies local structural fluctuation. In particular, one-dimensional (1D) systems have a propensity to be sensitive to these fluctuations as described by one of the maxims of condensed matter physics, *i.e.*, one chain does not make a crystal. Thus, the dynamical formation of active species and sites by these fluctuations is a key factor in establishing a microscopic model for chemical reactions at surfaces and nano-structured compounds. It is well known that the adsorption of O on Ag(110) results in the formation of quasi-1D structures, AgO chains, accompanied by the mass transfer of substrate atoms.

AgO chains arrange periodically to form (n×1) (n = 2 ~ 7) depending on the fractional O coverage due to repulsive interchain interactions. On the added-row reconstructed Ag(110) (n×1)-O surfaces, one-dimensional –Ag–O–Ag–O– chains arrange periodically. Scanning tunneling microscopy was used for studying spatiotemporal evolution of the disproportionation reaction of H_2O with O adatoms on oxidized Ag(110) surfaces where quasi-one dimensional AgO chains form ordered structures. Initially the reaction takes place slowly on Ag(110)-(5×1)O at the end of AgO chain, whereas the reaction accelerates explosively upon the appearance of a chemical wave that propagates along the direction perpendicular to the chain. The surface morphology of the region swept over by the chemical wave completely changes from (5×1)-O to that with many rectangular islands, indicating the formation of $H_2O(OH)_2$. The induction time and explosive acceleration with the propagating chemical wave imply that the reaction is autocatalytic. Water clusters hydrating OH produced likely play a central role in serving as a reservoir of H_2O to feed to the reaction and enhancing the reactivity of H_2O with O adatoms in AgO chains.

References

1) M. Fuyuki, K. Watanabe and Y. Matsumoto, *Phys. Rev. B* **74**, 195412 (6 pages) (2006).
2) Y. Matsumoto, *Bull. Chem. Soc. Jpn.* **80**, 842–855 (2007).
3) Y. Matsumoto and K. Watanabe, *Chem. Rev.* **106**, 4234–4260 (2006).
4) T. Matsumoto, *et al.*, *Surf. Sci.* doi:10.1016/j.susc.2007.04.157

* Present Address; Osaka University, The Institute of Scientific and Industrial Research, Osaka 567-0047

† Present Address; Kyoto University, Graduate School of Sciences, Department of Chemistry, Kyoto 606-8502

‡ Present Address; Genesis Research Institute, Inc. Chiba 272-0001

Visiting Professors

Visiting Professor
KITAJIMA, Masahiro *(from National Institute for Materials Science)*

Electron-Phonon Interaction Dynamics and Optical Control of the Coherent Optical Phonons

We are studying on coherent phonons in metals and semiconductors, using fs pump-probe techniques. Our main interest is to know how excited carriers are coupled with the phonons coherently. We have recently started investigating optical control of coherent phonons in semimetals by using a pair of fs laser pulses whose relative timing is tuned on the attosecond time scale. This new challenge is being collaborated with the Prof. Ohmori's group of IMS, and would serve as a powerful tool for understanding the fundamental mechanism of the interaction between a photo-excited single particle and the constituents of the surrounding lattice.

Visiting Associate Professor
BABA, Masaaki *(from Kyoto University)*

Excited-State Structure and Dynamics of Isolated Molecules

Excited-state dynamics such as internal conversion (IC) to the ground state, intersystem crossing (ISC) to the triplet state, intramolecular vibrational redistribution (IVR), and predissociation are of great interest because these radiationless transitions are closely related to the energy level scheme and break down of Born-Oppenheimer or adiabatic approximation. Rotationally resolved ultrahigh-resolution laser spectroscopy is powerful to investigate not only the accurate level energies, but also the lifetime, magnetic moment, and coherence of the isolated molecules in a supersonic jet. These properties are very important to understand the origin of dynamical processes in the electronic excited state.

Visiting Professor
SODA, Kazuo *(from Nagoya University)*

Electronic Structure of Bulk Metallic Glasses and Heusler-Type Alloys

The electronic structures and their correlation with functional properties of bulk metallic glasses and Heusler-type Fe-based alloys have been investigated by means of photoelectron spectroscopy and photoabsorption spectroscopy with use of synchrotron radiation as a light source in order to clarify the origins of their fascinating functional properties. Bulk metallic glasses is bulky multi-component amorphous alloys, possessing useful engineering properties in spite of their thermodynamically metastable phase, while Heusler-type Fe-based alloys are promising thermoelectric materials, showing high mechanical strength and larger power factor than a conventional Bi-Te semiconductors.

Visiting Associate Professor
OKADA, Kazumasa *(from Hiroshima University)*

Study on the Fragmentation of Molecules and Clusters in the Inner-Valence and Inner-Shell Electron Excitation Regions

The knowledge of the mechanisms involved in the ionization helps us to understand various processes in which there exists interaction of molecules and photons or electrons. The fragmentation dynamics of highly-excited or multiply-ionized molecules and clusters is studied by means of time-of-flight mass spectrometry. Multiple modes of measurement are used to obtain branching ratios of fragment ions or breakdown diagrams. Kinetic energy distribution of fragments provides insight into the nature of the fragmentation process.